Experimental demonstration of thermally tunable Fano and EIT resonances in coupled resonant system on SOI platform

Littlejohns, Callum George; Zhang, Zecen; Ng, Geok Ing; Hu, Ting; Qiu, Haodong; Guo, Xin; Wang, Wanjun; Liu, Chongyang; Sia, Jiaxu; Zhou, Jin; Nedeljkovic, Milos; Reed, Graham T.; Wang, Hong; Mohamed Saïd Rouifed

2018

Zhang, Z., Ng, G. I., Hu, T., Qiu, H., Guo, X., Wang, W., . . . Wang, H. (2018). Experimental demonstration of thermally tunable Fano and EIT resonances in coupled resonant system on SOI platform. IEEE Photonics Journal, 10(3), 6601108-. doi:10.1109/JPHOT.2018.2839621

https://hdl.handle.net/10356/105688

https://doi.org/10.1109/JPHOT.2018.2839621

Experimental Demonstration of Thermally Tunable Fano and EIT Resonances in Coupled Resonant System on SOI Platform

Zecen Zhang,[1] Geok Ing Ng,[1] Ting Hu,[1] Haodong Qiu,[1] Xin Guo,[1] Wanjun Wang,[1] Mohamed Saïd Rouifed,[1] Chongyang Liu,[1] Jiaxu Sia,[1] Jin Zhou,[1] Callum G. Littlejohns,[1, 2] Milos Nedeljkovic,[2] Graham T. Reed,[2] and Hong Wang [1]

[1]Silicon Technologies, Centre of Excellence, School of Electrical and Electronic Engineering, Nanyang Technological University, Singapore 639798
[2]Optoelectronics Research Centre, University of Southampton, Southampton SO17 1BJ, U.K.

DOI:10.1109/JPHOT.2018.2839621

Manuscript received April 23, 2018; revised May 17, 2018; accepted May 18, 2018. Date of publication May 22, 2018; date of current version June 18, 2018. This work was supported in part by the National Research Foundation Singapore under Grant NRF-CRP12-2013-04 and in part by the Nanyang Technological University-A*Star Silicon Technologies Centre of Excellence. Corresponding author: Geok Ing Ng (e-mail: EGING@ntu.edu.sg).

Abstract: Thermally tunable Fano and electromagnetically induced transparency (EIT) resonances are theoretically and experimentally demonstrated based on a Mach–Zehnder interferometer assisted Bragg grating-microring coupled resonant system on silicon-on-insulator (SOI) platform. In this paper, the destructive and constructive coupling between the two resonators, the microring resonator and the Fabry–Perot resonator formed by two Bragg gratings, give rise to the Fano and EIT resonances, respectively. The resonance lineshape can be controlled and converted by tuning the optical path length of the MZI arm. The device performance has been theoretically analyzed by using a specially developed numerical model. The coupled resonant system was designed, fabricated, and characterized on a commercial (SOI) platform. The tuning and conversion of the resonance lineshape by thermo-optical effect have been experimentally observed and verified, with good agreement between the experimental data and the simulations.

Index Terms: Silicon nanophotonics, integrated nanophotonic systems, electro-optical systems.

1. Introduction

Fano resonances, characterized by sharp asymmetric lineshape, have been widely utilized in communication [1]–[3] and biochemical sensing [4]–[6] applications. Electromagnetically induced transparency (EIT) resonances, by virtue of low insertion loss and high time delay, have attracted significant attentions in the applications of signal processing [7]–[9]. So far most efforts are focusing on either tunable Fano resonances or tunable EIT resonances [10]–[23]. However, limited research work has been reported on the system that can switch between Fano and EIT resonances. In 2006, the conversion between the Fano-like transmission and the multi-peaks transmission was reported

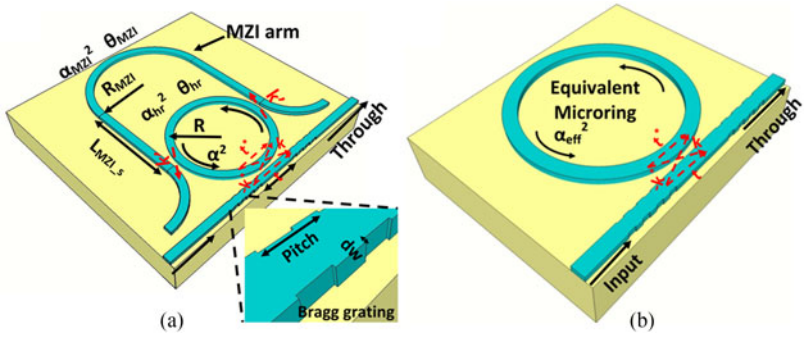

Fig. 1. (a) The schematic of the MZI-assisted Bragg grating-microring coupled resonant system. (b) The equivalent model of the MZI-assisted Bragg grating-microring coupled resonant system.

by W. Liang *et al.* through changing the coupling strength in a Fabry–Perot etalon-microtoroid resonator coupled system [24]. In 2009, the modifiable EIT-like and Fano-like transmissions were demonstrated by C.–H. Dong *et al.* based on the two-mode interference in a single silica microsphere by tuning the relative position of the fiber taper [25]. But for these two systems, the adoption of fiber techniques brings large feature sizes as well as the incompatibility with the planar waveguide fabrication process. If Fano and EIT resonances can be tuned and converted in a single on-chip system, the versatility, flexibility and compatibility can be much improved. And large volume integration on a single monolithic wafer then becomes possible. Recently, the conversion between Fano and EIT resonances was realized in an on-chip system consisting of a silicon ring resonator with two integrated tunable reflectors [26], [27]. But the reported system is not so compact as the footprint is more than 1000 μm* 400 μm, which is more than 330 times larger than the proposed system in this manuscript (30 μm*40 μm).

In this manuscript, thermally tunable Fano and EIT resonances are theoretically and experimentally demonstrated based on a Mach–Zehnder interferometer (MZI)-assisted Bragg grating-microring coupled resonant system on SOI platform. By changing the optical path length of the MZI arm, the effective round-trip power attenuation of the MZI-assisted microring can be tuned, which leads to the change of the coupling status between the two resonators. When the coupling changes between destructive and constructive status, the resonance lineshape is converted between Fano and EIT lineshape. We theoretically calculated and analyzed the performance of the system with a specially developed numerical model based on the transfer matrix method. The system was designed, fabricated and characterized on a commercial 220 nm-top-silicon-layer silicon-on-insulator (SOI) platform. The tuning and conversion between Fano and EIT resonances by thermo-optical effect have been experimentally observed and verified with good agreement between the experimental data and the simulations.

2. Device Designs and Simulations

The schematic of the MZI-assisted Bragg grating-microring coupled resonant system is shown in Fig. 1(a). Two Bragg gratings are located in the input-through bus waveguide at the two sides of the coupling region acting as two partially reflective elements to form a Fabry-Perot (F-P) resonator. In this work, the coupling between the resonances of the microring and the F-P resonator gives rise to the various EIT and Fano resonances. The two coupling points between the MZI arm and the microring are set at the two sides of the microring as shown in Fig. 1(a). L_{MZI_s} and R_{MZI} are the length of the straight section and the bending radius of the MZI arm respectively. The length of the MZI arm is defined as the total length between these two coupling points, which can be expressed as $L_{MZI} = 2 \cdot L_{MZI\_s} + \pi \cdot R_{MZI}$. The power attenuation coefficient and the phase shift of the MZI arm are ${\alpha_{MZI}}^2$ and θ_{MZI} respectively. Correspondingly, α_{hr}^2 and θ_{hr} are the power attenuation

coefficient and the phase shift of the half microring between the two coupling points. α^2 and R are the round-trip power attenuation coefficient and the radius of the microring resonator respectively. $t = \sqrt{1 - |k|^2}$ is the transmission coefficient of the coupling region between the input-through bus waveguide and the microring, and t^* is the conjugation. k is the coupling coefficient of the coupling region between the input-through bus waveguide and the microring, and k^* is the conjugation. k' is the coupling coefficient of the two coupling points between the MZI arm and the microring. pitch is the pitch of the Bragg gratings. dw is the depth of the corrugation. L_{cv} is the length of the F-P cavity, and N is the number of the periods of the Bragg gratings.

Based on the transfer matrix method, the transmission of the whole system can be expressed as [28]:

$$T_{input} = T_{Brag} \times T_{WG} \times T_{R\_eqv} \times T_{WG} \times T_{Brag} \times T_{output} \tag{1}$$

where the inverse expression is adopted; T_{Brag} is the matrix of the Bragg gratings; T_{WG} is the matrix of the straight waveguide; and T_{R_eqv} is the matrix of the equivalent microring resonator, which will be explained later. More detailed information can be found in [29].

In order to simplify the discussion, an add-drop bus waveguide with an effective coupling coefficient k_{eff} can be utilized to equivalently replace the MZI arm, where k_{eff} can be calculated by [30], [31]:

$$k_{eff}^2 = k'^2\left(1 - k'^2\right) \cdot \left(\alpha_{MZI}^2 + \alpha_{hr}^2 - 2\alpha_{MZI}\alpha_{hr}\cos\left(\theta_{MZI} - \theta_{hr}\right)\right) \tag{2}$$

while the relative phase $\Delta\theta = \theta_{MZI} - \theta_{hr}$ is changed from 0 to π, k_{eff}^2 can be tuned from 0 to $4k'^2(1 - k'^2)$. Furthermore, as shown in Fig. 1(b), by considering the equivalent add-drop bus waveguide and the microring as a single microring, the system can be further simplified as an all-pass microring coupled with an F-P resonator. The effective round-trip power attenuation of this equivalent single microring can be expressed as $\alpha_{\text{eff}}^2 = \alpha^2 - k_{eff}^2$. So, α_{eff}^2 can be tuned by changing $\Delta\theta$, which can be realized by changing the optical path length of the MZI arm by means of thermo-optical, electro-optical, or all-optical effects. In this experiment, the changing of the optical path length of the MZI arm is achieved by thermo-optical effect. Via tuning α_{eff}^2, the coupling status between the microring and the F-P resonator can be changed as well as the resonance lineshape. When $\alpha_{\text{eff}} > t$, the microring resonator operates in the over-coupling regime. The phase curve of the microring resonator is continuous and the coupling between the microring resonator and the F-P resonator is constructive, which results in the EIT peak. However, when $\alpha_{\text{eff}} = t$, the microring resonator operates at the critical-coupling point. An abrupt π shift of the microring phase curve occurs [32], and the coupling between the two resonators turns to completely destructive, which generates a sharp Fano lineshape with the largest extinction ratio (ER). When $\alpha_{\text{eff}} < t$, the microring resonator operates in the under-coupling regime. The phase shifting is maintained but with smaller values. The two light paths of the two resonators undergo partially destructive interference, which results in Fano lineshapes with smaller ERs. More detailed discussions can be referred in [33].

The simulations are conducted on a 220 nm-top-silicon-layer SOI platform with 2 μm buried oxide (BOX) layer, based on the transfer matrix method. For an initial design, we chose the parameters as $pitch = 315$ nm, $N = 100$, $dw = 10$ nm, $R = 10\ \mu$m, $R_{MZI} = 10.715\ \mu$m (the gap widths between the MZI arm and the microring are set as 115 nm), $k' = 0.4i$, $k = 0.45i$, $t = 0.8930$, $L_{cv} = 10.5 \cdot$ pitch. Since the simulations are conducted in a narrow band, the dispersion of the group index can be ignored and the value of the group index is set as 4.067. As shown in Fig. 2(a), the curve of α_{eff} is periodical. By heating up the MZI arm, the curve of α_{eff} is blue-shifted, which is consistent with [25]. $\Delta\varphi$ is the additional phase difference between the MZI arm and the half microring caused by the increased temperature of the MZI arm. The value of t is marked out with a horizontal black long-dashed line as 0.8930. When the curve of α_{eff} is blue-shifted, the value of α_{eff} at the wavelength of the Fano dip or EIT peak changes as well as the coupling status between the two resonators. The transmission spectra under different $\Delta\varphi$ are shown in Fig. 2(b). A magnified image of the black dashed-line circled region is presented in Fig. 2(c). As seen, when the MZI arm is at room temperature (red line), α_{eff} is much larger than t hence an EIT resonance is generated. While we

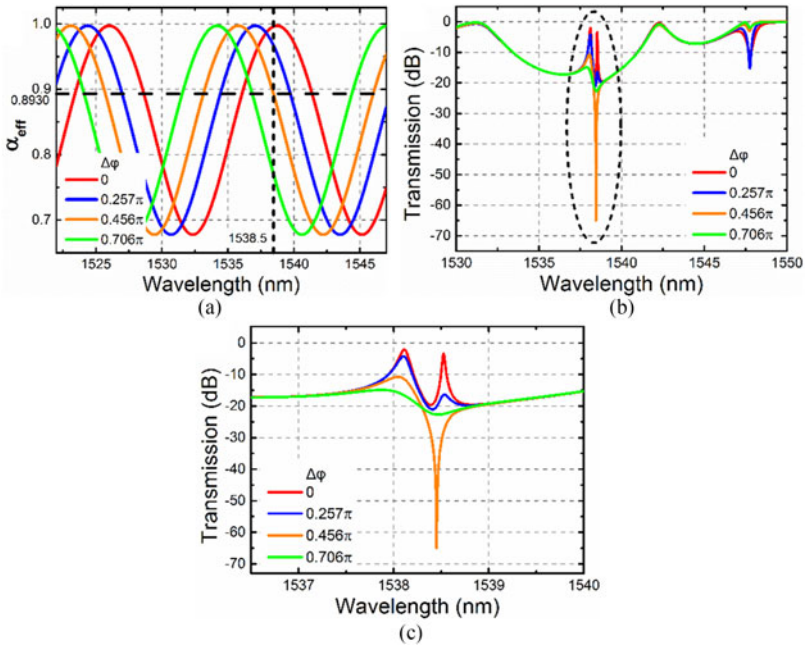

Fig. 2. (a) The curves of α_{eff} versus wavelength under different $\Delta\varphi$ when $t = 0.8930$. (b) The transmission spectra under different $\Delta\varphi$ when $t = 0.8930$. (c) The magnified spectra of the transmissions circled by the black dashed line in Fig. 2(b).

heat up the MZI arm to increase $\Delta\varphi$ from 0 to 0.257π (blue line), the ER of the EIT peak drops from 16.1 dB to 4.63 dB, and the insertion loss (IL) increases from 3.5 dB to 16.4 dB. At the same time, the full-width-at-half-maximum (FWHM) of the EIT peak becomes smaller from ~0.03 nm to ~0.213 nm, which corresponds to the decrease of the quality factor (Q factor) from ~51200 to ~7200. So while $\alpha_{\text{eff}} > t$ and with the decreasing difference between α_{eff} and t, the ER, the IL and the sharpness of the EIT peak are all degraded. For the application in a photonics integrated circuit, the IL can be fine-tuned to achieve an acceptable value and meet the requirement. When the temperature of the MZI arm is increased until $\Delta\varphi = 0.456\,\pi$, α_{eff} is equal to t and critical coupling occurs, which acts as a threshold point between Fano and EIT lineshapes. At that point, the transmission spectrum is converted from EIT lineshape to Fano lineshape. It is also noteworthy that the Fano resonance obtains the largest ER of 55 dB at the same time. When we continue raising the temperature of the MZI arm until $\Delta\varphi = 0.706\,\pi$, the Fano resonance lineshape remains but the ER significantly decreases to only 7.8 dB. Besides, the required wavelength shifting between the dip and the peak of the Fano lineshape also increases from ~0.405 nm to ~0.59 nm. So while $\alpha_{\text{eff}} \leq t$ and with the increasing difference between t and α_{eff}, not only the ER of the Fano resonance drops but also the sharpness degrades.

3. Device Fabrication and Characterizations

The fabricated device is shown in Fig. 3. The grating layer and the waveguide layer were both patterned with electron beam lithography (EBL). The grating layer was etched down to a depth of 70 nm with reactive ion etching (RIE). The waveguide layer was etched down to the BOX layer with deep reactive ion etching (DRIE). Then the sample was coated with a cladding layer of 1 μm SiO_2. A layer of 110 nm Ti was deposited and partially lifted off on the SiO_2 cladding to form the heating wires. Then a 20 nm Ti layer and a 300 nm Au layer were deposited. The metal at the patterned area is kept and the unwanted metal is lifted off to form the conducting wires and the electrode pads. The designed parameters were: pitch = 315 nm, $N = 100$, $dw = 15$ nm, $R = 10\,\mu$m,

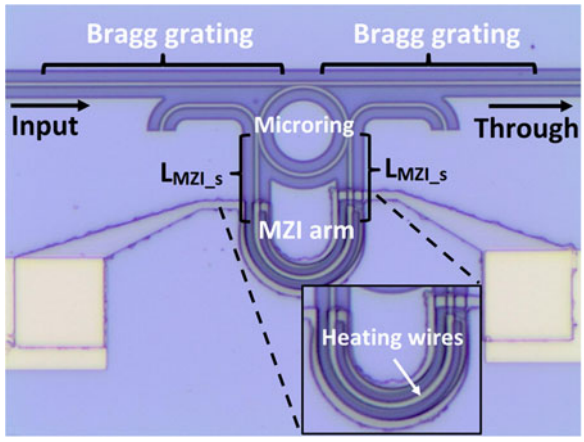

Fig. 3. The fabricated thermal-optic switch between Fano and EIT resonances based on a MZI-assisted Bragg grating-microring coupled system.

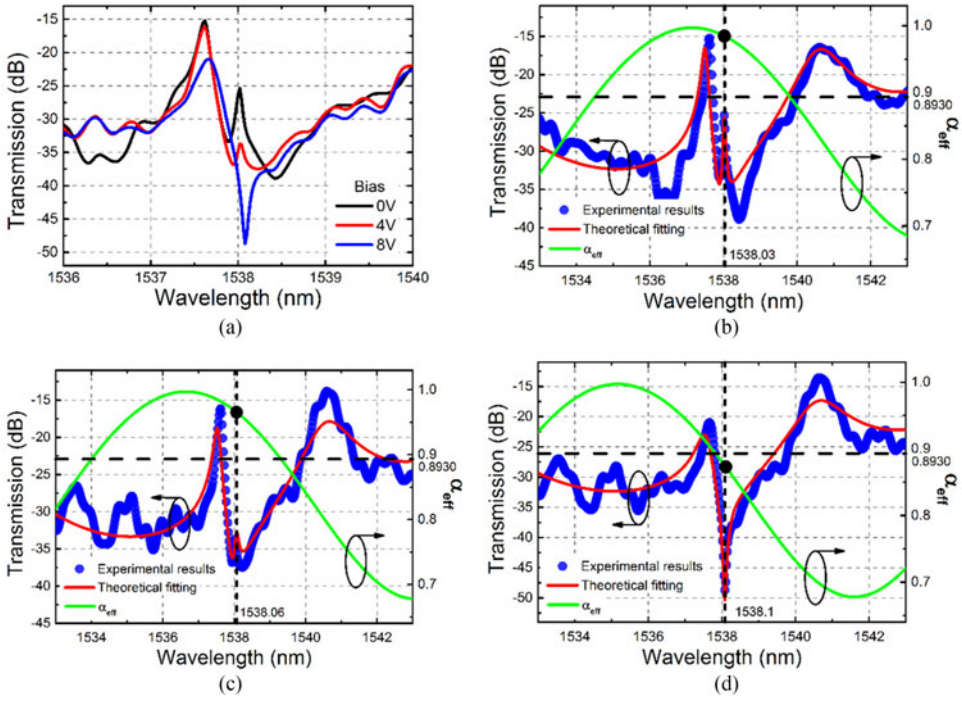

Fig. 4. (a) The experimental transmission spectra when the bias voltage is 0 V, 4 V and 8 V. (b) The fitted transmission spectrum when the bias voltage is 0 V and the corresponding curve of α_{eff}. (c) The fitted transmission spectrum when the bias voltage is 4 V and the corresponding curve of α_{eff}. (d) The fitted transmission spectrum when the bias voltage is 8 V and the corresponding curve of α_{eff}.

$R_{MZI} = 10.715\,\mu$m, $L_{cv} = 10.5 \cdot$ pitch. The gap widths between the MZI arm and the microring were set as 115 nm. The gap width between the input-through bus waveguide and the microring was 85 nm. The width of waveguide was 500 nm. L_{MZI_s} was 21.5 μm. The width of the Ti heating wires was 1.5 μm. Two specially designed grating couplers are applied at the input and output ports to couple light into and out from the system, which can also avoid the reflection caused by the ending of waveguide.

The experimental results under a series of bias voltages of 0 V, 4 V and 8 V are shown in Fig. 4(a). It can be clearly seen that while the bias voltage increases from 0 V to 8 V, the transmission spectrum

gradually converts from EIT lineshape to Fano lineshape. In Fig. 4(b)–(d), the experimental results of the bias voltage of 0V, 4 V and 8 V are fitted with our numerical model respectively and the corresponding curves of α_{eff} are also plotted. As seen, all the experimental results and the simulation results are in good agreement. Because the widths of the gaps are kept constant, the values of k and k' are fitted and fixed as 0.45i and 0.4i respectively in all these devices. Besides, in all the fittings, N, dw, R_{MZI} and pitch are kept constant and fitted as 100, 9.5 nm, 10.715 μm and 314.4 nm respectively. The difference between the designed value (15 nm) and fitted value (9.5 nm) of dw is because the fabricated corrugations of the Bragg grating are not in ideal rectangular shape. The fabricated Bragg gratings are comparable with the ideal rectangular Bragg grating with a corrugation depth of 9.5 nm. The value of t is marked as 0.8930 with horizontal black long-dashed lines and the wavelengths of the EIT peak or the Fano dip are marked with vertical black short-dashed lines. While the bias voltage increases from 0 V to 4 V, $\Delta\varphi$ increases from 0 to 0.077π and α_{eff} decreases from 0.9846 to 0.9654. In the meantime, the EIT resonance lineshape maintains but the ER of the EIT peak drops more than a half from 8.73 dB to 3.6 dB and the FWHM increases from $\sim$0.07 nm to $\sim$0.25 nm (corresponding to the decrease of Q factor from $\sim$21900 to $\sim$6150). Both the ER and the sharpness are degraded, which are in good agreement with the above simulations. Next, with the increase of bias voltage to 8 V, $\Delta\varphi$ increases from 0.077π to 0.308π as expected and α_{eff} drops from 0.9654 to 0.8716. As a result, the Fano transmission is generated. As measured, the ER is 27.4 dB and the required wavelength shifting between the dip and the peak is 0.557 nm. The small ripples of the curves are probably due to the weak optical reflection at the input and output facets. Besides, it is noteworthy that the wavelength of the EIT peak or the Fano dip is slightly red-shifted while the bias voltage increases. It is because the distance between the Ti heating wire and the microring waveguide is not large enough and the microring waveguide is also heated up by the heater, which results in the red-shifting of the microring resonance peak. The thermal isolation can be improved by etching deep trenches between the microring and the MZI arm. Alternatively, the additional phase difference $\Delta\varphi$ can be achieved by employing the phase-changing materials, such as VO_2 and $Ge_2Sb_2Te_5$ [34], [35]. At the same time, the influence on the performance and the lifetime of the device from the thermal heating wires can be avoided. Furthermore, the Bragg grating can be replaced by a Sagnac-loop mirror (SLM) [36] or an offset in the bus waveguide [37] for obtaining a broader operation bandwidth and ease the controlling of fabrication process. However, compared with the SLM, the Bragg grating is much more compact and suitable for high density integration. And the advantage of the Bragg grating over the offset in the bus waveguide is that, the transmission spectrum can be flexibly and conveniently tuned by changing parameters of the Bragg grating. So these three kinds of partially reflective elements can be utilized for the applications with different requirements.

4. Conclusion

In summary, a thermal-optic switch between Fano and EIT resonances is theoretically and experimentally demonstrated based on a MZI-assisted Bragg grating-microring coupled resonant system. In this work, the coupling between the MZI-assisted microring resonator and the F-P resonator gives rise to the EIT and Fano resonances. By changing the optical path length of the MZI arm, the resonant status of the MZI-assisted microring can be tuned as well as the resonance lineshape. The performance of the system is theoretically calculated and analyzed with a specially developed numerical model. Active tuning with thermo-optical effect is experimentally verified to be able to achieve the conversion of the resonance lineshape. The experimental and simulation results are in good agreement. With the capability of on-chip tuning and converting the resonance between Fano and EIT lineshapes, great improvements in the versatility, flexibility and compatibility of the system as well as the possibility of high volume monolithic integration become possible. As a result, it is envisaged that more related potential applications in communication, biochemical sensing and on-chip signal processing can be realized.

References

[1] W. Zhao, H. Jiang, B. Liu, Y. Jiang, C. Tang, and J. Li, "Fano resonance based optical modulator reaching 85% modulation depth," *Appl. Phys. Lett.*, vol. 107, no. 11, pp. 171109, Oct. 2015.

[2] N. K. Emani, T. Chung, A. V. Kildishev, V. M. Shalaev, Y. P. Chen, and A. Boltasseva, "Electrical modulation of fano resonance in plasmonic nanostructures using graphene," *Nano Lett.*, vol. 14, no. 1, pp. 78–82, Dec. 2014.

[3] M. Amin, R. Ramzan, and O. Siddiqui, "Fano resonance based ultra high-contrast electromagnetic switch," *Appl. Phys. Lett.*, vol. 110, no. 18, May 2017, Art. no. 181904.

[4] E. Semouchkina, R. Duan, G. Semouchkin, and R. Pandey, "Sensing based on fano-type resonance response of all-dielectric metamaterials," *Sensors*, vol. 15, no. 4, pp. 9344–9359, Apr. 2015.

[5] R. Singh, W. Cao, I. Al-Naib, L. Cong, and W. Withayachumnankul, "Ultrasensitive terahertz sensing with high-Q Fano resonances in metasurfaces," *Appl. Phys. Lett.*, vol. 105, no. 17, Oct. 2014, Art. no. 171101.

[6] Y. Gao, S. Zhan, Q. Liu, Y. Liu, "Controllable plasmonic sensing based on Fano resonance in a cavity coupled defective MDM waveguide," *Jour. Phys. D: Appl. Phys.*, vol. 49, no. 26, Jul. 2016, Art. no. 265109.

[7] M. Klein, M. Hohensee, Y. Xiao, R. Kalra, D. F. Phillips, and R. L. Walsworth, "Slow-light dynamics from electromagnetically-induced-transparency spectra," *Phys. Rev. A*, vol. 79, no. 5, May 2009, Art. no. 053833.

[8] A. H. Safavi-Naeini *et al.*, "Electromagnetically induced transparency and slow light with optomechanics," *Nature*, vol. 472, pp. 69–73, Apr. 2011.

[9] S. Kocaman, X. Yang, J. F. McMillan, M. B. Yu, D. L. Kwong, and C. W. Wong, "Observations of temporal group delays in slow-light multiple coupled photonic crystal cavities," *Appl. Phys. Lett.*, vol. 96, no. 22, Jun. 2010, Art. no. 221111.

[10] A. E. Miroshnichenko, S. Flach, and Yu. S. Kivshar, "Fano resonances in nanoscale structures," *Rev. Mod. Phys.*, vol. 82, no. 3, pp. 2257–2298, Jun. 2009.

[11] M. Galli, S. L. Portalupi, M. Belotti, L. C. Andreani, L. O'Faolain, and T. F. Krauss, "Light scattering and Fano resonances in high-Q photonic crystal nanocavities," *Appl. Phys. Lett.*, vol. 94, no. 7, Feb. 2009, Art. no. 071101.

[12] A. C. Ruege and R. M. Reano, "Multimode waveguides coupled to single mode ring Resonators," *J. Lightw. Technol.*, vol. 27, no. 12, pp. 2035–2043, Jun. 2009.

[13] K. K. Mehta, J. S. Orcutt, and R. J. Ram, "Fano line shapes in transmission spectra of silicon photonic crystal resonators," *Appl. Phys. Lett.*, vol. 102, no. 8, Feb. 2013, Art. no. 081109.

[14] Q. Huang, Z. Shu, G. Song, J. Chen, J. Xia, and J. Yu. "Electromagnetically induced transparency-like effect in a two-bus waveguides coupled microdisk resonator," *Opt. Exp.*, vol. 22, no. 3, pp. 3219–3227, Feb. 2014.

[15] W.-S. Chang *et al.*, "A plasmonic fano switch," *Nano Lett.*, vol. 12, no. 9, pp. 4977–4982, Aug. 2012.

[16] Z. Chai, X. Hu, C. Li, H. Yang, Q. Gong, "On-chip multiple electromagnetically induced transparencies in photon−plasmon composite nanocavities," *ACS Photon.*, vol. 3, no. 11, pp. 2068–2073, Oct. 2016.

[17] T. Hu *et al.*, "Tunable Fano resonances based on two-beam interference in microring resonator," *Appl. Phys. Lett.*, vol. 102, no. 1, Jan. 2013, Art. no. 011112.

[18] S. Liu, M. Zhang, W. Wang, and Y. Wang, "Tuning multiple Fano resonances in plasmonic pentamer clusters," *Appl. Phys. Lett.*, vol. 102, no. 13, Apr. 2013, Art. no. 133105.

[19] G. Zhao *et al.*, "Tunable Fano resonances based on microring resonator with feedback coupled waveguide," *Opt. Exp.*, vol. 24, no. 18, pp. 20187–20195, Sep. 2016.

[20] W. Zhang, W. Li, and J. Yao, "Optically tunable Fano resonance in a grating based Fabry–Perot cavity-coupled microring resonator on a silicon chip," *Opt. Lett.*, vol. 41, no. 11, pp. 2474–2477, Jun. 2016.

[21] H. Xiao *et al.*, "Tunable Fano resonance in mutually coupled micro-ring resonators," *Appl. Phys. Lett.*, vol. 111, no. 9, Aug. 2017, Art. no. 091901.

[22] S. Han, L. Cong, H. Lin, B. Xiao, H. Yang, and R Singh, "Tunable electromagnetically induced transparency in coupled three-dimensional split-ring resonator metamaterials," *Sci. Rep.*, vol. 6, Feb. 2016, Art. no. 20801.

[23] P. Shi, G. Zhou, J. Deng, F. Tian, and F. S. Chau, "Tuning all-optical analog to electromagnetically induced transparency in nanobeam cavities using nanoelectromechanical system," *Sci. Rep.*, vol. 5, Sep. 2015, Art. no. 14379.

[24] W. Liang, L. Yang, J. K. S. Poon, Y. Huang, K. J. Vahala, and A. Yariv, "Transmission characteristics of a Fabry–Perot etalon–microtoroid resonator coupled system," *Opt. Lett.*, vol. 31, no. 4, pp. 510–512, Feb. 2006.

[25] C.-H. Dong, C.-L. Zou, Y.-F. Xiao, J.-M. Cui, Z.-F. Han, and G.-C. Guo, "Modified transmission spectrum induced by two-mode interference in a single silica microsphere," *J. Phys. B*, vol. 42, no. 21, Nov. 2009, Art. no. 215401.

[26] A. Li and W. Bogaerts, "An actively controlled silicon ring resonator with a fully tunable Fano resonance," *APL Photon.*, vol. 2, Sep. 2017, Art. no. 096101.

[27] A. Li and W. Bogaerts, "Tunable electromagnetically induced transparency in integrated silicon photonics circuit," *Opt. Exp.*, vol. 25, no. 25, pp. 31688–31695, Dec. 2017.

[28] L. Chrostowski, V. M. Hochberg, *Silicon Photonics Design from Devices to Systems*, Cambridge, U.K: Cambridge Univ., 2015.

[29] Z. Zhang, G. I. Ng, T. Hu, H. Qiu, X. Guo, M. S. Rouifed, C. Liu, and H. Wang, "Electromagnetically induced transparency-like effect in microring-Bragg gratings based coupling resonant system," *Opt. Exp.*, vol. 24, no. 12, pp. 25665–25675, Oct. 2016.

[30] L. Chen, N. Sherwood-Droz, and M. Lipson, "Compact bandwidth-tunable microring resonators," *Opt. Lett.*, vol. 32, no. 22, pp. 3361–3363, Nov. 2007.

[31] H. L. Lira, C. B. Poitras, and M. Lipson, "CMOS compatible reconfigurable filter for high bandwidth non-blocking operation," *Opt. Exp.*, vol. 19, no. 21, pp. 20115–20121, Oct. 2011.

[32] W. Bogaerts *et al.*, "Silicon microring resonators," *Laser Photon. Rev.*, vol. 6, no. 1, pp. 47–73, Jan. 2012.

[33] Z. Zhang *et al.*, "Conversion between EIT and Fano spectra in a microring-Bragg grating coupled-resonator system," *Appl. Phys. Lett.*, vol. 111, no. 8, Aug. 2017, Art. no. 081105.

[34] S. Cueff *et al.*, "Dynamic control of light emission faster than the lifetime limit using VO2 phase-change," *Nat. Commun.*, vol. 6, Oct. 2015, Art. no. 8636.

[35] A. B. Pevtsova, A. N. Poddubny, S. A. Yakovlev, D. A. Kurdyukov, and V. G. Golubev, "Light control in $Ge_2Sb_2Te_5$-coated opaline photonic crystals mediated by interplay of Wood anomalies and 3D Bragg diffraction," *J. Appl. Phy.*, vol. 113, no. 14, Apr. 2013, Art. no. 144311.
[36] S. Zheng *et al.*, "Compact tunable electromagnetically induced transparency and Fano resonance on silicon platform," *Opt. Exp.*, vol. 25, no. 21, pp. 25655–25662, Oct. 2017.
[37] C. -Y. Chao and L. J. Guo, "Biochemical sensors based on polymer microrings with sharp asymmetrical resonance," *Appl. Phys. Lett.*, vol. 83, no. 8, pp. 1527–1529, Aug. 2003.